Room-Temperature Spin-Transport Properties in an $In_{0.5}Ga_{0.5}As$ Quantum Dot Spin-Polarized Light-Emitting Diode

Kohei Etou, Satoshi Hiura,* Soyoung Park, Kazuya Sakamoto, Junichi Takayama, Agus Subagyo, Kazuhisa Sueoka, and Akihiro Murayama

Faculty of Information Science and Technology, Hokkaido University, Kita 14, Nishi 9, Kita-ku, Sapporo 060-0814, Japan

(Received 22 January 2021; revised 29 March 2021; accepted 17 June 2021; published 14 July 2021)

An understanding of the spin-transport properties in semiconductor barriers is essential to improve the performance of spin-polarized light-emitting diodes (spin LEDs) for future optospintronics integration in information processing. Here, we report on the temperature and bias-voltage dependence of spin-transport properties in an $In_{0.5}Ga_{0.5}As$ quantum dot (QD) spin LED using a combination of spin-dependent electroluminescence (EL) and time-resolved photoluminescence. The QD EL spin polarization increases with an increase in temperature above 125 K; this is attributed to the improved conversion efficiency from spin polarization of electrons to circular polarization of photons of the QDs. We find that both the electric field and temperature can enhance spin relaxation in the undoped GaAs barrier above 200 K. At 298 K, the QD EL spin polarization decreases beyond 2.5 V; this is attributed to the enhanced D'yakonov Perel' spin relaxation in the undoped GaAs barrier caused by the increase in electron temperature. This study provides valuable insights into the spin-relaxation mechanism in the semiconductor barrier during the room-temperature operation of the QD spin LED.

DOI: 10.1103/PhysRevApplied.16.014034

I. INTRODUCTION

In recent years, optospintronics has attracted considerable research attention because of its potential applications in information technology and in an understanding of the fundamental physics of electron spins in condensed matter [1]. The optical transfer of spin information of carriers in solid-state circuits is important for optical interconnections in future optospintronics integrations in information processing. Spin-polarized light-emitting diodes (spin LEDs) and laser diodes that can directly convert electron spins into circularly polarized light have been extensively studied by employing III-V semiconductor quantum wells (QWs) [2–14] and quantum dots (QDs) [15–21] as active layers. QDs are the most promising material in the active layer because of their significant suppression of carrier-spin relaxation and temperature-independent luminescence properties that originate from the strong three-dimensional quantum confinement [22–26]. For a spin LED, circularly polarized light, reflecting the spin polarization of carriers injected from spin injectors, is emitted based on the optical-transition selection rule in semiconductor active layers [27]. Dominant depolarization for spin-polarized carriers can occur in transport barriers between the spin injector and the emissive layers. A large decrease in spin polarization from 31% at the MnAs spin injector to 6% at the InAs QDs has been reported at 200 K [18]. At high temperatures, spin relaxation in transport barriers is accelerated because of the well-known D'yakonov–Perel' (DP) mechanism [28]. A decrease in electroluminescence (EL) spin polarization with an increasing bias voltage is observed over a wide temperature range of 10–300 K [6,9,21]. Thus, a thorough understanding of the effect of temperature and bias voltage on the spin-transport properties in spin LEDs is required to achieve a better performance to ensure stable operations at room temperature.

Here, we investigate the temperature and bias-voltage dependence of the spin-transport properties in QD spin LEDs via a combination of circularly polarized EL and time-resolved photoluminescence (TRPL). Although the systematic temperature and bias-voltage dependence of the EL spin polarization for the QD spin LED has been studied recently [21], the previous study was conducted only at low temperatures below 110 K. This study focuses on EL spin-polarization properties at temperatures above 125 K and provides a comprehensive understanding of the effect of temperature and bias voltage on the spin-transport properties in the spin LED that have not been adequately explored. We find that the spin relaxation in the undoped GaAs barrier mainly influences the EL spin-polarization properties at room temperature.

*hiura@ist.hokudai.ac.jp

II. EXPERIMENTAL DETAILS

Figure 1(a) shows a schematic of the QD spin LED. The multilayered structure is grown by molecular beam epitaxy for the semiconductor, while the tunnel barrier and the ferromagnetic electrode are grown by electron-beam (EB) evaporation. The *p*-*i*-*n* LED device has the following sequence: *p*-GaAs : Zn (100) substrate ($p = 1 \times 10^{19}$ cm^{-3})/*p*-GaAs : Be($p = 1 \times 10^{18}$ cm^{-3}, 350 nm)/*p*-$Al_{0.15}Ga_{0.85}As$: Be($p = 1 \times 10^{18}$ cm^{-3}, 50 nm)/undoped GaAs(40 nm)/active layer/*n*-$Al_{0.1}Ga_{0.9}As$: Si ($n = 2 \times 10^{17}$ cm^{-3}, 50 nm)/*n*-GaAs : Si($n = 2 \times 10^{17}$ cm^{-3}, 5 nm). The active layer comprises three layers of 7.5-monolayer-(ML) thick $In_{0.5}Ga_{0.5}As$ QDs, with an areal density of 1.6×10^{10} cm^{-2}, and an average diameter of 27 nm [see Fig. 1(b)]. Each QD layer is capped with a 10-nm-thick *p*-doped GaAs barrier ($p = 6 \times 10^{17}$ cm^{-3}) and another 30-nm-thick undoped GaAs barrier. After growth of the semiconductor part, the sample is transferred to the EB chamber without air exposure to grow a 3-nm-thick MgO tunnel barrier at 573 K. Then, the sample is transferred in air to another EB chamber to grow a 10-nm-thick Fe electrode after cleaning the MgO surface by annealing at 573 K for 30 min under an oxygen atmosphere of 7×10^{-5} Pa. Finally, standard photolithography and etching are performed to fabricate a conventional LED device; no noticeable leakage currents are detected. The size of the contact area on the device is 0.35×0.35 mm^2.

Circularly polarized EL and PL are measured at 125–298 K by mounting the spin LED device in a superconducting magnet cryostat with a maximum magnetic field of 5 T normal to the sample plane. An injection current is changed from 1 to 10 mA. The EL and PL signals are detected using an (In, Ga)As detector (Andor, iDus 1.7 μm) in the Faraday geometry. The polarization-resolved TRPL is measured using a streak camera (Hamamatsu Photonics, C10910-02) combined with a spectrometer (Hamamatsu Photonics, C11119-04) under σ^+-polarized excitation over the same temperature range. A mode-locked Ti:sapphire pulsed laser with a repetition rate of 80 MHz and a pulse width of less than 100 fs is used as the excitation source. The

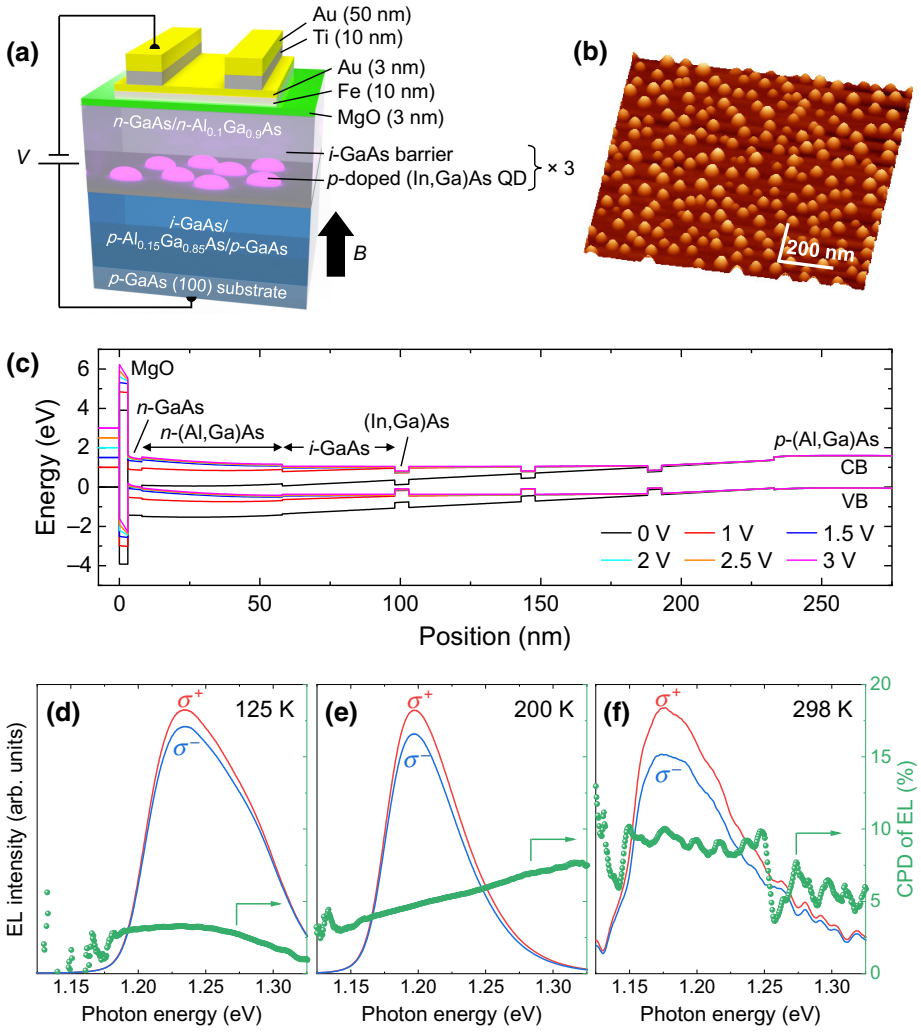

FIG. 1. (a) Schematic of QD spin LED. (b) Atomic force microscopy image of $In_{0.5}Ga_{0.5}As$ QDs grown under the same conditions as those in this study. (c) One-dimensional calculation of band structure for spin LED at various bias voltages at 298 K. Circularly polarized QD EL spectra and corresponding CPD measured at (d) 125 K, (e) 200 K, and (f) 298 K with 4 mA at $B = 5$ T.

excitation energy is tuned to 1.55 eV to generate spin-polarized carriers in the undoped GaAs barriers. Here, the polarization of electron spins generated in the barriers is expected to be 50%, according to the optical-transition selection rule [27]. The circular polarization degree (CPD) of EL and PL is analyzed through the combination of a quarter-wave plate with a linear polarizer defined a CPD $= (I_{\sigma+} - I_{\sigma-})/(I_{\sigma+} + I_{\sigma-})$, where $I_{\sigma\pm}$ denotes the circularly polarized EL and PL intensities. The CPD measured in QDs directly reflects the electron-spin polarization at QD emissive states because hole spins are rapidly depolarized in a barrier before injection into QDs [29,30].

III. RESULTS AND DISCUSSION

Figure 1(c) shows the calculated band structure at various bias voltages for the spin LED at 298 K using NEXTNANO software [31]. For simplification of calculations, the layer of $In_{0.5}Ga_{0.5}As$ QD is modeled by a 5-nm-thick $In_{0.5}Ga_{0.5}As$ quantum well. For layers other than the QD layer, the nominal thicknesses, material compositions, and doping concentrations are used as parameters in the simulation. Below 1.5 V, the applied bias mainly drops on the semiconductor part, and then holes are accumulated at the interface between MgO and semiconductor. Above 1.5 V, the applied bias starts to drop on the MgO layer, which results in band bending in the MgO barrier. It should be noted that the band structure of the (In, Ga)As layer is almost unchanged from 1.5 to 3.0 V. This result indicates that the effect of bias voltage on the optical properties of the QDs, such as emission energy and radiative recombination rate, are negligible over this bias-voltage range. Another feature of the spin LED is that the (In, Ga)As-based active layer is sandwiched between the (Al, Ga)As barriers, which behave as electron-blocking layers. The electron spins electrically injected into the semiconductor layer from the Fe electrode are confined in the active layer, and thus, sufficiently strong luminescence of the QDs at high temperatures can be expected.

Figures 1(d)–1(f) show circularly polarized EL spectra of the QDs and the corresponding CPDs measured at 125, 200, and 298 K with an injection current of 4 mA under a magnetic field of 5 T. All spectra exhibit a predominant luminescence from the QD ground state (GS), as in a previous study [15]. The EL peak appears at around 1.24 eV at 125 K and shifts to about 1.20 and 1.18 eV at 200 and 298 K, respectively. Here, the net In composition of this (In, Ga)As QD is estimated via three-dimensional quantum simulations using NEXTNANO software [31]. We find that the GS transition energy of 1.18 eV at 298 K corresponds to the $In_{0.4}Ga_{0.6}As$ QDs (for details, see Sec. A of the Supplemental Material [32]). The lower In composition than the nominal one can be attributed to In desorption and In-Ga intermixing during the capping process of the QDs [33]. The redshift of the QD emission is caused by the decreased QD band gap with increasing temperature. A slight peak at around 1.30 eV appears at 125 K. This feature can be attributed to enhancement of the emission from the QD excited states (ESs) by a strong p-doping effect [34]. The high-energy shoulder becomes considerably weaker at 200 K, which is probably caused by the dominant thermal escape of electrons from the QD ESs [35]. This feature appears again at around 1.23 eV at 298 K, and it can be explained by the thermal population of electrons at high temperatures [15].

These EL spectra shown in Figs. 1(d)–1(f) exhibit differences between σ^+ and σ^- components, i.e., nonzero CPD values reflect the electron-spin polarization in the QDs. At 125 K, the CPD of 3% is observed at a peak energy that corresponds to the QD GS. The CPD value increases to 5% at 200 K and then to 10% at 298 K. Here, the Zeeman effect on the observed CPD properties is extremely small because the Zeeman splitting of less than 1 meV for (In, Ga)As QDs at 5 T [36–38] is negligible compared with the thermal energy at these high temperatures. A previous study of the InAs QD spin LED using an Fe electrode as a spin injector shows no Zeeman effect on the EL CPD properties from 120 to 300 K [15]. Another property to affect the measured EL CPD is the magnetic circular dichroism (MCD), which causes a different absorption of left and right circularly polarized light through the ferromagnetic layer [13,39]. The MCD effect can artificially increase the CPD values. Here, we find that the MCD effect from our spin LED is estimated to be less than 0.1% (for details, see Sec. B of the Supplemental Material [32]).

Figure 2(a) shows the EL spectra measured at 298 K under various bias voltages from 2.2 to 3.0 V, corresponding to injection currents from 3 to 10 mA. We observe no change in the peak energy with bias voltage. This result indicates that there is no quantum-confined Stark effect [40] influencing the QD's emission properties. The injection-current dependence of the integrated EL intensity is presented in Fig. 2(b). The EL intensity exponentially increases with increasing injection current, which means that the external quantum efficiency (EQE) becomes higher. This behavior is in sharp contrast to a previous report on the (In, Ga)As QD-based spin LED measured at 10 K [21], which shows a decreased EQE with increasing injection current due to the state-filling effect in QDs [41]. Here, notably, state filling in QDs can be strongly suppressed as the temperature increases above 100 K [42]. Furthermore, for larger injection currents (bias voltages), the transfer time of electrons in the transport barrier can be reduced, and thus, the number of electrons trapped in nonradiative defects or recombined radiatively during transport is likely to decrease. Therefore, we anticipate that the suppressed state filling in QDs and the increased number of electrons injected into the QDs contribute to

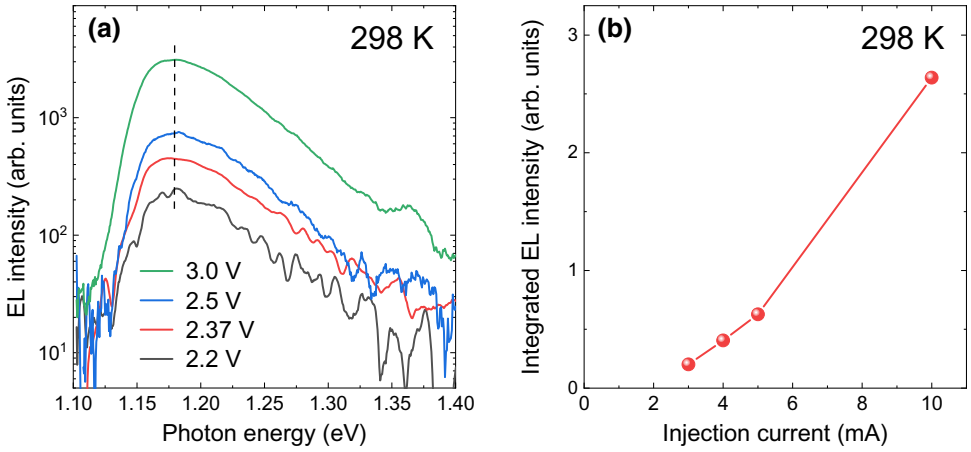

FIG. 2. (a) EL spectra measured under various bias voltages at 298 K with $B = 5$ T. Dashed line indicates constant peak energy independent of bias voltage. (b) Integrated EL intensity as a function of injection current at 298 K with $B = 5$ T.

the observed exponential increase in the EL intensity with increasing injection current at 298 K.

Figure 3(a) shows the magnetic field dependence of the average EL CPD of the QD GS with 0.3 mA at 150 K. In this study, the QD GS is defined as an energy range of 1.22–1.26 eV at 125 K. The analyzed energy range of a QD GS is shifted with a change in temperature, according to Varshni's law using the parameters of $In_{0.5}Ga_{0.5}As$ [43]. The CPD increases rapidly with the magnetic field up to about 2 T, corresponding to the saturation magnetic field of Fe [3]. Above 2 T, the CPD slowly continues to increase with magnetic field. It is well known that a large magnetic field can suppress the DP spin relaxation in GaAs [44], which causes a positive linear background of the measured EL CPD [6,45]. Based on these previous reports, the slow increase in EL CPD above 2 T can be attributed to the magnetic-field-induced background. This linear background should be subtracted to evaluate the net EL CPD properties. The CPD increase rates of 0.35 and 0.28%/T are obtained in the positive and negative magnetic field directions, respectively, by a simple linear-fit analysis. The linear background can be estimated as 0.32%/T (average of these two values). The magnetic field dependence of the average EL CPD of the QD GS with 4 mA at 298 K is shown in Fig. 3(b). The estimated linear background of 0.32%/T follows the slow increase in EL CPD above 2 T well, considering the standard deviation (error bar) of data points. Therefore, it is valid that the EL CPD values presented here are corrected by subtraction of this linear background (0.32%/T). Hereafter, the net EL CPD values after subtraction of the linear background are given.

Figure 3(c) shows the net average EL CPD of the QD GS as a function of the magnetic field at 298 K. The net EL CPD tracks the simplified hard-axis magnetization curve of Fe (not experimental data), which is roughly normalized to the maximum CPD (see the dashed line). The saturation magnetic field is determined by the magnetic properties of Fe, $4\pi M = 2.2$ T [3]. This result clearly indicates that the observed EL CPD properties are derived from the electrical injection of electron spins from the Fe electrode. The CPD value saturates at a value of approximately 8% when the Fe magnetization is fully out of the plane. Since the spin polarization of Fe is around 40% [46], the spin-to-photon conversion efficiency of this spin LED, which is defined by the ratio of the EL CPD to the spin polarization of the spin injector, can be estimated as 20% at 298 K.

Figure 3(d) shows the net average EL CPDs of the QD GS as functions of temperature with various injection currents. Here, data measured above 200 K with 1 mA and at 298 K with 2 mA are not plotted, because a sufficient emission intensity from the QDs is not detected. Below 4 mA, the CPD value gradually increases with temperature, while the increase in CPD becomes weaker at 6 mA above 200 K. At 8 mA, the CPD value decreases slightly above 250 K. Therefore, the large difference in the EL CPD behavior between injection currents appears above 200 K. To understand these complex CPD behaviors as functions of temperature and injection current (bias voltage), one needs to extract the degree of spin conservation in the three-dimensional transport barriers and conversion efficiency from spin polarization of electrons to circular polarization of photons of the QDs separately. In general, the net EL spin polarization of the QD spin LED at a fixed injection current can be defined as [21]

$$P_{\mathrm{EL}}(T) = P_{\mathrm{FM}} D_{\mathrm{tr}}(T) \eta_{\mathrm{QD}}(T), \tag{1}$$

where P_{FM} denotes the spin polarization of the ferromagnetic electrode and D_{tr} denotes the degree of the spin conservation in the transport barrier. η_{QD} represents the conversion efficiency from spin polarization of electrons to circular polarization of photons of the QDs; it is determined by the PL decay time, τ_r, and spin-relaxation time, τ_s, in the QDs as [35]

$$\eta_{\mathrm{QD}} = (1 + \tau_r/\tau_s)^{-1}. \tag{2}$$

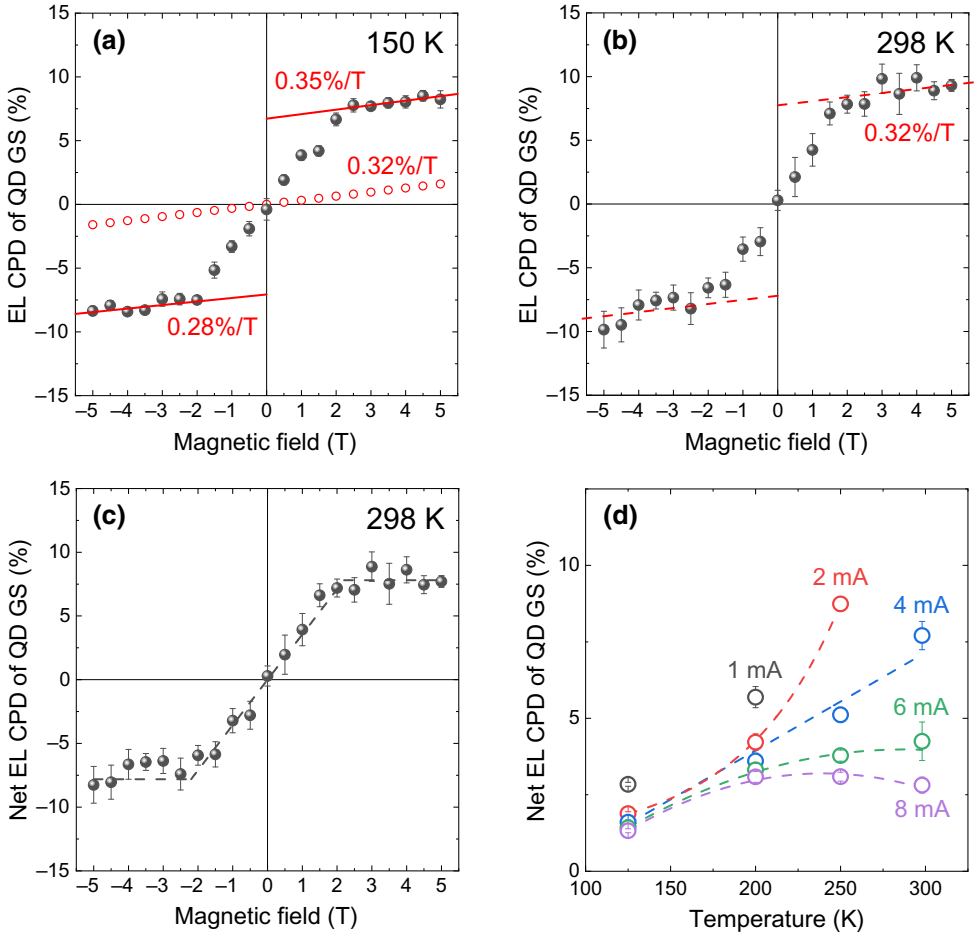

FIG. 3. (a) Magnetic field dependence of EL CPD of QD GS with 0.3 mA at 150 K. Red solid lines indicate linear fitting results from 2.5 to 5 T. Red open circles show estimated linear background. Magnetic field dependence of EL CPD of QD GS with 4 mA at 298 K (b) before and (c) after subtraction of linear background. Estimated linear background of 0.32%/T follows slow CPD increase above 2 T [see red dashed lines in (b)]. Gray dashed line in (c) indicates simplified hard-axis magnetization curve of Fe (not experimental data) with a saturation field of 2.2 T [3], which is roughly normalized to the maximum CPD. (d) Net EL CPD of QD GS as a function of temperature with various injection currents at $B = 5$ T. Dashed lines indicate guidelines for each injection current.

Equation (1) indicates that the net D_{tr} can be obtained by investigating the temperature dependence of η_{QD} because $P_{\mathrm{FM}} = 40\%$ for Fe is constant.

Figures 4(a) and 4(b) show circularly polarized PL time profiles and corresponding CPDs of the QD GS at 200 and 298 K, respectively, with conditions of zero bias and zero magnetic field. The excitation power is set to 0.5 mW to obtain the net η_{QD} without the state-filling effect in QDs (for details, see Sec. C of the Supplemental Material [32]). Here, the CPD decay time constant corresponds to half of the electron-spin-relaxation time, τ_s, in a conventional spin-split two-level system [47]. The resulting τ_s at 298 K is (441 ± 21) ps, compared with (500 ± 15) ps at 200 K. The temperature dependence of τ_s is summarized in Fig. 4(c), which exhibits an almost constant τ_s with temperature. This result clearly demonstrates that the discrete density of states and the spatial localization of carriers in the QDs inhibit both the DP and phonon-scattering processes, which reduce τ_s at high temperatures [18]. The large decrease in τ_r from 1.5 ns at 200 K to 0.2 ns at 298 K is observed as shown in Figs. 4(a) and 4(b). Figure 4(c) shows the monotonic decrease in τ_r with increasing temperature above 175 K. Here, τ_r can be expressed by the radiative (τ_{rad}) and nonradiative (τ_{nr}) decay processes, as follows [42]:

$$1/\tau_r = 1/\tau_{\mathrm{rad}} + 1/\tau_{\mathrm{nr}}, \tag{3}$$

where τ_{nr} includes thermal excitation (escape) of carriers, trapping by defects and impurities, and dark-exciton formation. The decrease in τ_r with temperature is mainly due to the decrease in τ_{nr} because of the strong thermal escape of the electrons from the QD GS at high temperatures [48]. Figure 4(d) shows η_{QD} as a function of temperature; these are obtained using τ_s and τ_r based on Eq. (2). η_{QD} drastically increases from 18% at 150 K to 69% at 298 K because of the temperature-independent spin-relaxation time unique to the QDs compared with the significant decrease in the PL decay time, as described above. Here, η_{QD} is expected to be almost independent of injection current and bias voltage (for details, see Secs. C and D of the Supplemental Material [32]). The magnetic field (Zeeman) effect on η_{QD} should be negligible because the thermal energy at temperatures above 100 K is much higher than the Zeeman splitting of less than 1 meV for (In, Ga)As QDs at 5 T [36–38]. Therefore, we anticipate that η_{QD} depends only on temperature. These results

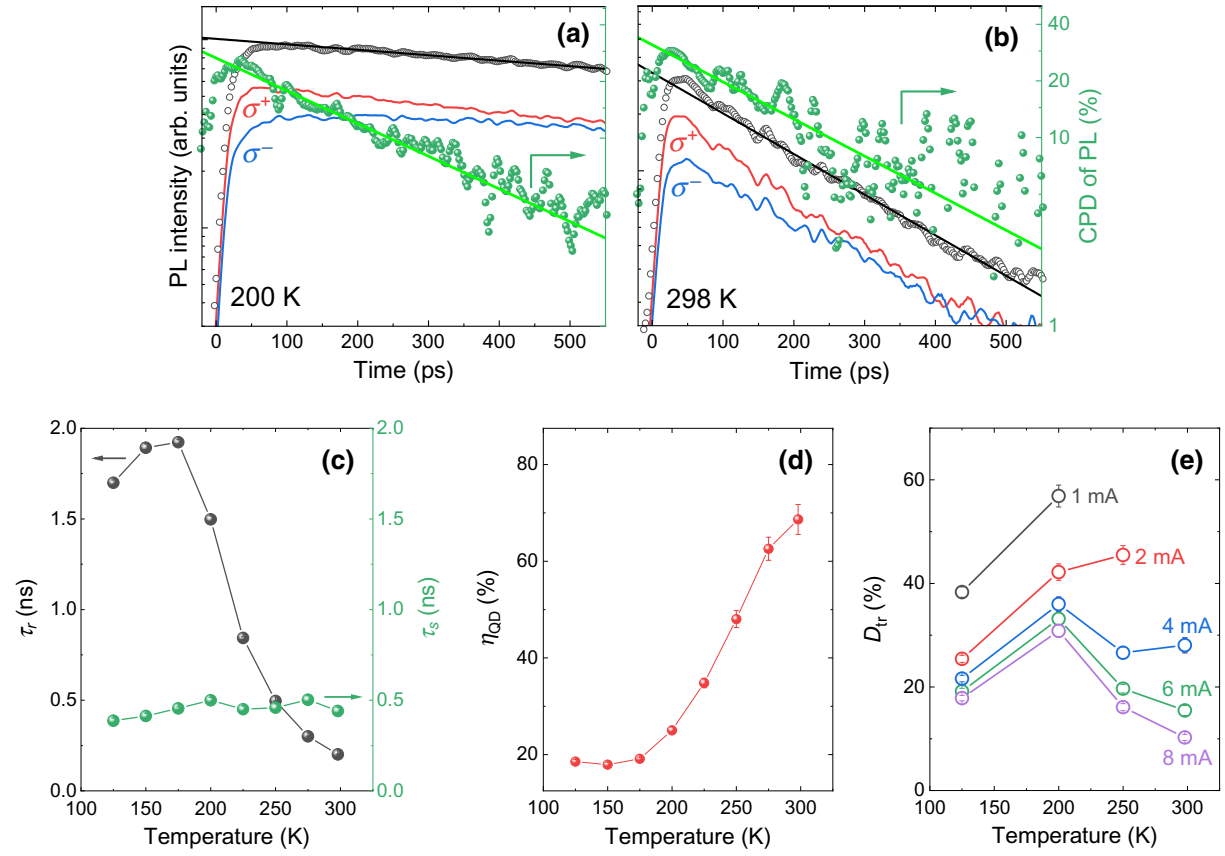

FIG. 4. Circularly polarized TRPL and corresponding CPD of the QD GS at (a) 200 K and (b) 298 K with $B = 0$ T. Green solid lines indicate single-exponential decay fittings for time-dependent CPD. Sum of $\sigma^{\pm}$-polarized PL intensity as a function of time (black open circles) with single-exponential decay fittings (black solid lines) is shown. (c) PL decay time, τ_r, and spin-relaxation time, τ_s, of QDs as functions of temperature. (d) Conversion efficiency from spin polarization of electrons to circular polarization of photons of QDs, η_{QD} as a function of temperature. (e) Degree of spin conservation during transport, D_{tr}, as functions of temperature with various injection currents.

indicate that the observed higher EL CPD at higher temperatures [see Figs. 1(d)–1(f)] can be mainly attributed to the improved conversion efficiency from spin polarization of electrons to circular polarization of photons of the QDs.

Figure 4(e) shows the degree of spin conservation during transport, D_{tr}, as a function of temperature with various injection currents obtained using $P_{FM} = 40\%$ for Fe and $\eta_{QD}(T)$ shown in Fig. 4(d) based on Eq. (1). The increases in D_{tr} between 125 and 200 K are observed for all injection currents. In general, under a high electric field, a population of electrons may be driven out of thermal equilibrium with the crystal lattice; hence, the electron temperature becomes higher than the lattice temperature [49]. The electrons slightly above the Fermi level can be accelerated by the external electric field, in addition to slight modifications of the conduction band for the transport barrier. This increase in the kinetic energy can enhance the electron temperature, while being suppressed by electron scattering. Spin depolarization in the transport barrier can be enhanced due to DP spin relaxation as a result of the electric-field-induced increase in the electron temperature [50]. For a constant injection current, the bias voltage applied on this spin LED decreases when the temperature increases (Fig. S10 within the Supplemental Material [32]). This means that the applied electric field in the transport barrier decreases as the temperature increases from 125 to 200 K. Therefore, the increases in D_{tr} between 125 and 200 K for all injection currents can be attributed to weakening of the electric-field-induced DP spin relaxation, which is caused by a decrease in the electron temperature.

On the other hand, the increases in D_{tr} between 125 and 200 K with an almost constant bias voltage are also observed (Fig. S11 within the Supplemental Material [32]). The obtained D_{tr} is likely to depend on the transit time of electrons in the transport barriers. The decrease in the transit time can reduce the possibility of spin flipping due to the DP mechanism before electrons reach the active layer [21]. A previous study of the single-crystal diamond has shown an abnormal decrease in the electron transit time between 125 and 200 K [51]. Therefore, we

deduce that both weakening of the electric-field-induced DP spin relaxation and a decrease in the electron transit time in the transport barrier are responsible for the increases in D_{tr} between 125 and 200 K. In contrast, D_{tr} largely decreases above 200 K at injection currents above 4 mA. This behavior can be explained by the enhancement of the temperature-induced DP spin relaxation. Because the rate of spin relaxation in the bulk is proportional to T^3 [52], we anticipate that the temperature-induced DP spin relaxation becomes dominant above 200 K.

Furthermore, Fig. 4(e) shows a systematic decrease in D_{tr} with the injection current (bias voltage), regardless of the temperature. To reveal its origin, we measure the circularly polarized PL under bias voltage with no magnetic field. Figure 5(a) shows the PL CPD spectra of QDs with various bias voltages at 298 K under excitation of the undoped GaAs barrier (excitation energy is set to 1.49 eV), where the EL components are subtracted using data measured without laser irradiation. The bias voltage is changed from 2.1 to 3.0 V, which corresponds to the change in injection currents from 2 to 10 mA. At 2.2 and 2.4 V, the PL CPD of nearly 15% appears at the QD GS around 1.18 eV, while it largely decreases to nearly 8% at 3.0 V. In general, the state-filling effect in the QDs induced by the increase in electron spins injected into the QDs can reduce the PL CPD values of the QDs [53–55]. The relative increase in the PL intensity from the QD ES with increasing bias voltage, which reflects the presence of state filling in the QD GS, is not observed from the bias-voltage dependence of the PL spectra [see the upper inset in Fig. 5(a)]. Therefore, the CPD decrease in the QD GS with bias voltage cannot be attributed to the state-filling effect in the QDs.

Another possible mechanism includes the decrease in η_{QD} with bias voltage or the bias-voltage-induced spin relaxation in the transport barrier. Here, as described above, η_{QD} is expected to be almost constant with bias voltage (injection current). Therefore, we conclude that the main origin is the decreased polarization of electron spins injected into the QDs caused by acceleration of the electric-field-induced DP spin relaxation in the transport barriers. Figures 5(b) and 5(c) show the bias-voltage dependence of the net EL and PL CPDs of the QD GS at 298 K. A clear correlation between these behaviors can be observed; however, the absolute values are different. Both exhibit the CPD decrease beyond 2.5 V, which indicates the presence of the threshold bias voltage of the CPD properties. Therefore, the electric-field-induced DP spin relaxation becomes dominant in the transport barrier above 2.5 V. Furthermore, this finding can be confirmed in Fig. 4(e), which shows a large decrease in D_{tr} from 28% at 4 mA (~2.4 V) to 10% at 8 mA (~2.8 V). These results clearly demonstrate that both the electric field and temperature play important roles in the spin-transport properties at temperatures above 200 K.

Finally, we discuss the transport barrier where spin relaxation is dominant. We evaluate spin relaxation in the $Al_{0.1}Ga_{0.9}As$ barrier by comparing the PL CPD of the QD GS under the excitation of $Al_{0.1}Ga_{0.9}As$ with that under the excitation of undoped GaAs. If spin relaxation is dominant in the $Al_{0.1}Ga_{0.9}As$ barrier, the measured PL CPD for the former case should be clearly lower. Figure 5(d) shows the bias-voltage dependence of the PL CPD of the QD GS at 298 K under the excitation of $Al_{0.1}Ga_{0.9}As$ (excitation energy is set to 1.65 eV). Similar behavior of the CPD values to that in the case of GaAs excitation is observed. These results indicate that spin relaxation in the GaAs barrier, not in the $Al_{0.1}Ga_{0.9}As$ barrier, mainly contribute to the decreased polarization of electron spins injected into the QDs, as shown in the lower inset in Fig. 5(a). Here, we deduce that spin relaxation can be

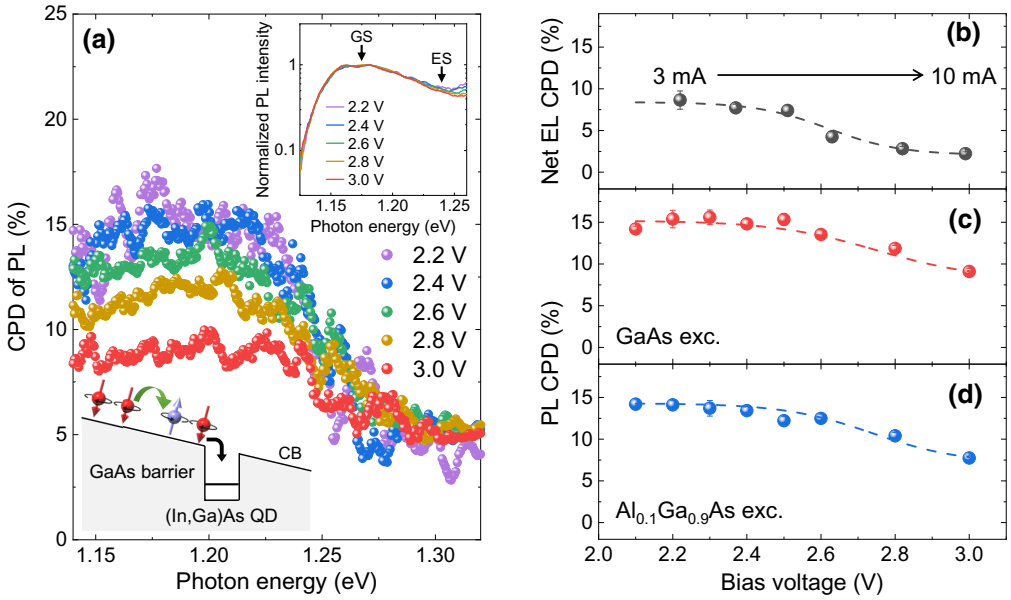

FIG. 5. (a) PL CPD spectra of QDs at various bias voltages at 298 K with $B = 0$ T under excitation of undoped GaAs barrier. Upper inset shows bias-voltage dependence of normalized QD PL spectra. Lower inset shows schematic of electron-spin relaxation in undoped GaAs barrier under high bias voltage. (b) Net EL CPD and PL CPD of QD GS at 298 K as a function of bias voltage under excitation of (c) undoped GaAs barrier and (d) $Al_{0.1}Ga_{0.9}As$ barrier. Dashed lines indicate guidelines.

suppressed in the p-doped GaAs barrier capping the QDs. It has been experimentally reported that the DP spin relaxation in the 10-nm-thick p-doped GaAs barrier capping the (In, Ga)As QDs can be potentially weakened through electron-impurity scattering at temperatures above 200 K [34]. Therefore, we conclude that spin relaxation is dominant in the undoped GaAs barrier. The band-structure simulation of the spin LED indicates that the applied electric field in the undoped GaAs barrier exceeds 0.5 kV/cm at 2.8 V (Fig. S12 within the Supplemental Material [32]). Based on a previous report, spin depolarization in GaAs can be accelerated above 0.5 kV/cm [56]. These findings clearly demonstrate that the performance of the QD spin LED strongly depends on the degree of electron-spin relaxation in the transport barrier, and it varies with temperature and bias voltage.

IV. CONCLUSION

We investigate the temperature and bias-voltage dependence of the spin-transport properties in QD spin LED via combined measurements of circularly polarized EL and TRPL. The net EL CPD of the QD GS increases from 2% at 125 K to 8% at 298 K. We attribute this behavior to the temperature-independent spin-relaxation time unique to the QDs, compared with the significant decrease in the PL decay time with temperature. Furthermore, we reveal that the spin-relaxation mechanism in the transport barrier is both temperature and bias dependent. Above 200 K, both the electric field and temperature play important roles in spin relaxation in the undoped GaAs barrier. At 298 K, the EL CPD of the QD GS decreases beyond 2.5 V; this is attributed to the enhanced DP spin relaxation in the undoped GaAs barrier. These results demonstrate that the combined measurements of circularly polarized EL and TRPL are effective to gain a quantitative understanding of the spin-transport properties in the spin LED. The findings of this study have significant implications for future developments of spin LEDs, as this study paves the way for a separation analysis of the electron-spin relaxation properties of the semiconductor transport barrier and the emissive layer. Finally, we emphasize that the EL spin polarization can be enhanced using a material with a longer spin relaxation than that of GaAs as a transport barrier. Dilute nitride Ga(N, As) is one such promising material because it can turn the nonmagnetic semiconductor into an efficient spin filter operating at room temperature and zero magnetic field [57].

ACKNOWLEDGMENTS

This work is supported by the Japan Society for the Promotion of Science (JSPS) under Grants No. 16H06359, No. 19K15380, No. 19H05507, and No. 21H01356. This work is also supported by the JST FOREST Program (Grant No. JPMJFR202E). Part of this work was conducted at the Hokkaido University, supported by "Nanotechnology Platform Program" of the Ministry of Education, Culture, Sports, Science and Technology (MEXT), Japan, Grant No. JPMXP09F20HK0010.

[1] I. Žutić, J. Fabian, and S. Das Sarma, Spintronics: Fundamentals and applications, Rev. Mod. Phys. **76**, 323 (2004).

[2] R. Fiederling, M. Keim, G. Reuscher, W. Ossau, G. Schmidt, A. Waag, and L. W. Molenkamp, Injection and detection of a spin-polarized current in a light-emitting diode, Nature **402**, 787 (1999).

[3] A. T. Hanbicki, B. T. Jonker, G. Itskos, G. Kioseoglou, and A. Petrou, Efficient electrical spin injection from a magnetic metal/tunnel barrier contact into a semiconductor, Appl. Phys. Lett. **80**, 1240 (2002).

[4] T. Manago and H. Akinaga, Spin-polarized light-emitting diode using metal/insulator/semiconductor structures, Appl. Phys. Lett. **81**, 694 (2002).

[5] A. T. Hanbicki, O. M. J. van 't Erve, R. Magno, G. Kioseoglou, C. H. Li, B. T. Jonker, G. Itskos, R. Mallory, M. Yasar, and A. Petrou, Analysis of the transport process providing spin injection through an Fe/AlGaAs Schottky barrier, Appl. Phys. Lett. **82**, 4092 (2003).

[6] X. Jiang, R. Wang, R. M. Shelby, R. M. Macfarlane, S. R. Bank, J. S. Harris, and S. S. P. Parkin, Highly Spin-Polarized Room-Temperature Tunnel Injector for Semiconductor Spintronics Using MgO(100), Phys. Rev. Lett. **94**, 056601 (2005).

[7] M. Holub, J. Shin, S. Chakrabarti, and P. Bhattacharya, Electrically injected spin-polarized vertical-cavity surface-emitting lasers, Appl. Phys. Lett. **87**, 091108 (2005).

[8] M. Holub, J. Shin, D. Saha, and P. Bhattacharya, Electrical Spin Injection and Threshold Reduction in a Semiconductor Laser, Phys. Rev. Lett. **98**, 146603 (2007).

[9] T. Manago, A. Sinsarp, and H. Akinaga, Growth condition dependence of spin-polarized electroluminescence in Fe/MgO light-emitting diodes, J. Appl. Phys. **102**, 083914 (2007).

[10] Y. Lu, V. G. Truong, P. Renucci, M. Tran, H. Jaffrès, C. Deranlot, J.-M. George, A. Lemaître, Y. Zheng, D. Demaille, P.-H. Binh, T. Amand, and X. Marie, Mgo thickness dependence of spin injection efficiency in spin-light emitting diodes, Appl. Phys. Lett. **93**, 152102 (2008).

[11] R. Farshchi, M. Ramsteiner, J. Herfort, A. Tahraoui, and H. T. Grahn, Optical communication of spin information between light emitting diodes, Appl. Phys. Lett. **98**, 162508 (2011).

[12] P. Barate, S. Liang, T. T. Zhang, J. Frougier, M. Vidal, P. Renucci, X. Devaux, B. Xu, H. Jaffrès, J. M. George, X. Marie, M. Hehn, S. Mangin, Y. Zheng, T. Amand, B. Tao, X. F. Han, Z. Wang, and Y. Lu, Electrical spin injection into InGaAs/GaAs quantum wells: A comparison between MgO tunnel barriers grown by sputtering and molecular beam epitaxy methods, Appl. Phys. Lett. **105**, 012404 (2014).

[13] S. H. Liang, *et al.*, Large and robust electrical spin injection into GaAs at zero magnetic field using an ultrathin CoFeB/MgO injector, Phys. Rev. B **90**, 085310 (2014).

[14] B. S. Tao, P. Barate, J. Frougier, P. Renucci, B. Xu, A. Djeffal, H. Jaffrès, J.-M. George, X. Marie, S. Petit-Watelot, S. Mangin, X. F. Han, Z. G. Wang, and Y. Lu, Electrical spin injection into GaAs based light emitting diodes using perpendicular magnetic tunnel junction-type spin injector, Appl. Phys. Lett. **108**, 152404 (2016).

[15] C. H. Li, G. Kioseoglou, O. M. J. van 't Erve, M. E. Ware, D. Gammon, R. M. Stroud, B. T. Jonker, R. Mallory, M. Yasar, and A. Petrou, Electrical spin pumping of quantum dots at room temperature, Appl. Phys. Lett. **86**, 132503 (2005).

[16] S. Chakrabarti, M. A. Holub, P. Bhattacharya, T. D. Mishima, M. B. Santos, M. B. Johnson, and D. A. Blom, Spin-polarized light-emitting diodes with Mn-doped InAs quantum dot nanomagnets as a spin aligner, Nano Lett. **5**, 209 (2005).

[17] L. Lombez, P. Renucci, P. F. Braun, H. Carrère, X. Marie, T. Amand, B. Urbaszek, J. L. Gauffier, P. Gallo, T. Camps, A. Arnoult, C. Fontaine, C. Deranlot, R. Mattana, H. Jaffrès, J.-M. George, and P. H. Binh, Electrical spin injection into p-doped quantum dots through a tunnel barrier, Appl. Phys. Lett. **90**, 081111 (2007).

[18] D. Basu, D. Saha, C. C. Wu, M. Holub, Z. Mi, and P. Bhattacharya, Electrically injected InAs/GaAs quantum dot spin laser operating at 200 K, Appl. Phys. Lett. **92**, 091119 (2008).

[19] P. Bhattacharya, A. Das, D. Basu, W. Guo, and J. Heo, An electrically injected quantum dot spin polarized single photon source, Appl. Phys. Lett. **96**, 101105 (2010).

[20] F. Cadiz, *et al.*, Electrical initialization of electron and nuclear spins in a single quantum dot at zero magnetic field, Nano Lett. **18**, 2381 (2018).

[21] A. E. Giba, X. Gao, M. Stoffel, X. Devaux, B. Xu, X. Marie, P. Renucci, H. Jaffrès, J.-M. George, G. Cong, Z. Wang, H. Rinnert, and Y. Lu, Spin Injection and Relaxation in p-Doped (In, Ga)As/GaAs Quantum-dot Spin Light-Emitting Diodes at Zero Magnetic Field, Phys. Rev. Appl. **14**, 034017 (2020).

[22] M. Paillard, X. Marie, P. Renucci, T. Amand, A. Jbeli, and J. M. Gérard, Spin Relaxation Quenching in Semiconductor Quantum Dots, Phys. Rev. Lett. **86**, 1634 (2001).

[23] P. Borri, W. Langbein, S. Schneider, U. Woggon, R. Sellin, D. Ouyang, and D. Bimberg, Ultralong Dephasing Time in InGaAs Quantum Dots, Phys. Rev. Lett. **87**, 157401 (2001).

[24] J. M. Elzerman, R. Hanson, L. H. Willems van Beveren, B. Witkamp, L. M. K. Vandersypen, and L. P. Kouwenhoven, Single-shot read-out of an individual electron spin in a quantum dot, Nature **430**, 431 (2004).

[25] A. I. Tartakovskii, J. Cahill, M. N. Makhonin, D. M. Whittaker, J.-P. R. Wells, A. M. Fox, D. J. Mowbray, M. S. Skolnick, K. M. Groom, M. J. Steer, and M. Hopkinson, Dynamics of Coherent and Incoherent Spin Polarizations in Ensembles of Quantum Dots, Phys. Rev. Lett. **93**, 057401 (2004).

[26] M. Kroutvar, Y. Ducommun, D. Heiss, M. Bichler, D. Schuh, G. Abstreiter, and J. J. Finley, Optically programmable electron spin memory using semiconductor quantum dots, Nature **432**, 81 (2004).

[27] F. Meier and B. P. Zakharchenya, *Optical Orientation* (Elsevier, North-Holland, Amsterdam, 1984).

[28] M. I. D'yakonov and V. I. Perel. Zh. Eksp. Teor. Fiz. **65**, 362 (1973). [Optical orientation in a system of electrons and lattice nuclei in semiconductors. Theory Sov. Phys. JETP **38**, 177 (1974)].

[29] D. J. Hilton and C. L. Tang, Optical Orientation and Femtosecond Relaxation of Spin-Polarized Holes in GaAs, Phys. Rev. Lett. **89**, 146601 (2002).

[30] S. Cortez, O. Krebs, S. Laurent, M. Senes, X. Marie, P. Voisin, R. Ferreira, G. Bastard, J.-M. Gérard, and T. Amand, Optically Driven Spin Memory in n-Doped InAs-GaAs Quantum Dots, Phys. Rev. Lett. **89**, 207401 (2002).

[31] S. Birner, T. Zibold, T. Andlauer, T. Kubis, M. Sabathil, A. Trellakis, and P. Vogl, Nextnano: General purpose 3-D simulations, IEEE Trans. Electron Devices **54**, 2137 (2007).

[32] See the Supplemental Material at https://link.aps.org/supplemental/10.1103/PhysRevApplied.16.014034 for a three-dimensional quantum simulation of QDs, the MCD effect on the measured EL CPD, injection-current and bias-voltage dependence of CE_{QD}, I-V curves of the LED sample at various temperatures, D_{tr} as a function of bias voltage, and the calculated electric field in the undoped GaAs barrier.

[33] T. Kaizu, T. Matsumura, and T. Kita, Broadband control of emission wavelength of InAs/GaAs quantum dots by GaAs capping temperature, J. Appl. Phys. **118**, 154301 (2015).

[34] S. Sato, S. Hiura, J. Takayama, and A. Murayama, Suppression of thermally excited electron-spin relaxation in InGaAs quantum dots using p-doped capping layers toward enhanced room-temperature spin polarization, Appl. Phys. Lett. **116**, 182401 (2020).

[35] S. Hiura, M. Takishita, J. Takayama, S. Sato, and A. Murayama, Highly Efficient Room-Temperature Electron-Photon Spin Conversion Using a Semiconductor Hybrid Nanosystem with Gradual Quantum Dimensionality Reduction, Phys. Rev. Appl. **14**, 044011 (2020).

[36] M. Bayer, G. Ortner, O. Stern, A. Kuther, A. A. Gorbunov, A. Forchel, P. Hawrylak, S. Fafard, K. Hinzer, T. L. Reinecke, S. N. Walck, J. P. Reithmaier, F. Klopf, and F. Schäfer, Fine structure of neutral and charged excitons in self-assembled In(Ga)As/(Al)GaAs quantum dots, Phys. Rev. B **65**, 195315 (2002).

[37] T. Nakaoka, T. Saito, J. Tatebayashi, and Y. Arakawa, Size, shape, and strain dependence of the g factor in self-assembled In(Ga)As quantum dots, Phys. Rev. B **70**, 235337 (2004).

[38] T. Nakaoka, T. Saito, J. Tatebayashi, S. Hirose, T. Usuki, N. Yokoyama, and Y. Arakawa, Tuning of g-factor in self-assembled In(Ga)As quantum dots through strain engineering, Phys. Rev. B **71**, 205301 (2005).

[39] S. T. Ruggiero, A. Williams, C. E. Tanner, S. Potashnik, J. Moreland, and W. H. Rippard, Magneto-optic effects in spin-injection devices, Appl. Phys. Lett. **82**, 4599 (2003).

[40] D. A. B. Miller, D. S. Chemla, T. C. Damen, A. C. Gossard, W. Wiegmann, T. H. Wood, and C. A. Burrus, Band-edge Electroabsorption in Quantum Well Structures: The Quantum-Confined Stark Effect, Phys. Rev. Lett. **53**, 2173 (1984).

[41] V. K. Kalevich, M. Paillard, K. V. Kavokin, X. Marie, A. R. Kovsh, T. Amand, A. E. Zhukov, Y. G. Musikhin,

V. M. Ustinov, E. Vanelle, and B. P. Zakharchenya, Spin redistribution due to Pauli blocking in quantum dots, Phys. Rev. B **64**, 045309 (2001).

[42] T. Kiba, X. Yang, T. Yamamura, Y. Kuno, A. Subagyo, K. Sueoka, and A. Murayama, Temperature dependence of the dynamics of optical spin injection in self-assembled InGaAs quantum dots, Appl. Phys. Lett. **103**, 082405 (2013).

[43] S. Paul, J. B. Roy, and P. K. Basu, Empirical expressions for the alloy composition and temperature dependence of the band gap and intrinsic carrier density in $Ga_xIn_{1-x}As$, J. Appl. Phys. **69**, 827 (1991).

[44] V. A. Marushchak, M. N. Stepanova, and A. N. Titkov, Suppression by a longitudinal magnetic field of spin relaxation of conduction electrons in semiconductor crystals lacking an inversion center, JETP Lett. **37**, 400 (1983).

[45] H. Höpfner, C. Fritsche, A. Ludwig, A. Ludwig, F. Stromberg, H. Wende, W. Keune, D. Reuter, A. D. Wieck, N. C. Gerhardt, and M. R. Hofmann, Magnetic field dependence of the spin relaxation length in spin light-emitting diodes, Appl. Phys. Lett. **101**, 112402 (2012).

[46] R. Allenspach, M. Taborelli, and M. Landolt, Oxygen on Fe(100): An Initial-Oxidation Study by Spin-Polarized Auger Spectroscopy, Phys. Rev. Lett. **55**, 2599 (1985).

[47] A. Tackeuchi, R. Ohtsubo, K. Yamaguchi, M. Murayama, T. Kitamura, T. Kuroda, and T. Takagahara, Spin relaxation dynamics in highly uniform InAs quantum dots, Appl. Phys. Lett. **84**, 3576 (2004).

[48] J. Beyer, I. A. Buyanova, S. Suraprapapich, C. W. Tu, and W. M. Chen, Strong room-temperature optical and spin polarization in InAs/GaAs quantum dot structures, Appl. Phys. Lett. **98**, 203110 (2011).

[49] M. P. Vaughan, *Hot Electron Transport* (Springer, Berlin, Heidelberg, 2012).

[50] M. I. Miah, Spin-drift transport in semiconductors, J. Phys. D: Appl. Phys. **41**, 035105 (2008).

[51] H. Jansen, D. Dobos, T. Eisel, H. Pernegger, V. Eremin, and N. Wermes, Temperature dependence of charge carrier mobility in single-crystal chemical vapour deposition diamond, J. Appl. Phys. **113**, 173706 (2013).

[52] R. S. Britton, T. Grevatt, A. Malinowski, R. T. Harley, P. Perozzo, A. R. Cameron, and A. Miller, Room temperature spin relaxation in GaAs/AlGaAs multiple quantum wells, Appl. Phys. Lett. **73**, 2140 (1998).

[53] S. Hiura, K. Takeishi, M. Urabe, K. Itabashi, J. Takayama, T. Kiba, K. Sueoka, and A. Murayama, Interdot spin transfer dynamics in laterally coupled excited spin ensemble of high-density InGaAs quantum dots, Appl. Phys. Lett. **113**, 023104 (2018).

[54] S. Hiura, S. Saito, J. Takayama, T. Kiba, and A. Murayama, Layer-selective spin amplification in size-modulated quantum nanocolumn, Appl. Phys. Lett. **115**, 013102 (2019).

[55] S. Hiura, S. Hatakeyama, J. Takayama, and A. Murayama, Asymmetric spin relaxation induced by residual electron spin in semiconductor quantum-dot-superlattice hybrid nanosystem, Appl. Phys. Lett. **116**, 262407 (2020).

[56] H. Sanada, I. Arata, Y. Ohno, Z. Chen, K. Kayanuma, Y. Oka, F. Matsukura, and H. Ohno, Relaxation of photoinjected spins during drift transport in GaAs, Appl. Phys. Lett. **81**, 2788 (2002).

[57] X. J. Wang, I. A. Buyanova, F. Zhao, D. Lagarde, A. Balocchi, X. Marie, C. W. Tu, J. C. Harmand, and W. M. Chen, Room-temperature defect-engineered spin filter based on a non-magnetic semiconductor, Nat. Mater. **8**, 198 (2009).